

## Accepted Manuscript

Polydopamine coated graphene oxide for anticorrosive reinforcement of water-borne epoxy coating

Mingjun Cui, Siming Ren, Haichao Zhao, Qunji Xue, Liping Wang

PII: S1385-8947(17)31896-X  
DOI: <https://doi.org/10.1016/j.cej.2017.10.172>  
Reference: CEJ 17956

To appear in: *Chemical Engineering Journal*

Received Date: 6 July 2017  
Revised Date: 29 October 2017  
Accepted Date: 30 October 2017

Please cite this article as: M. Cui, S. Ren, H. Zhao, Q. Xue, L. Wang, Polydopamine coated graphene oxide for anticorrosive reinforcement of water-borne epoxy coating, *Chemical Engineering Journal* (2017), doi: <https://doi.org/10.1016/j.cej.2017.10.172>

This is a PDF file of an unedited manuscript that has been accepted for publication. As a service to our customers we are providing this early version of the manuscript. The manuscript will undergo copyediting, typesetting, and review of the resulting proof before it is published in its final form. Please note that during the production process errors may be discovered which could affect the content, and all legal disclaimers that apply to the journal pertain.



## Polydopamine coated graphene oxide for anticorrosive reinforcement of water-borne epoxy coating

Mingjun Cui<sup>a,b,1</sup>, Siming Ren<sup>a,b,1</sup>, Haichao Zhao<sup>a\*</sup>, Qunji Xue<sup>a</sup>, Liping Wang<sup>a\*</sup>

<sup>a</sup>Key Laboratory of Marine Materials and Related Technologies, Zhejiang Key Laboratory of Marine Materials and Protective Technologies, Ningbo Institute of Materials Technology and Engineering, Chinese Academy of Sciences, Ningbo 315201, P. R. China

<sup>b</sup>University of Chinese Academy of Sciences, Beijing 100039, China

### Abstract

This study reports an eco-friendly water-borne epoxy (EP) with enhanced corrosion protection performance by embedding graphene oxide (GO). For this purpose, the dispersion of the GO in ethanol is improved by modifying the GO nanosheets with hydrophilic dopamine (DA), owing to the  $\pi$ - $\pi$  interactions between the GO and self-polymerized polydopamine (PDA) as well as the covalent bonding between DA and GO. Results obtained from transmittance electron microscopy (TEM), scanning probe microscopy (SPM) Fourier transform infrared (FT-IR) spectroscopy, Raman spectroscopy, UV-vis absorbance spectroscopy and X-ray photoelectron spectroscopy (XPS) reveal the successful modification of PDA on the surface of GO nanosheets. Besides, the GO/EP and GO-PDA/EP coatings are applied on the steel substrates and their corrosion protection performance is investigated via electrochemical measurements, scanning electron microscopy (SEM) and scanning vibration electrochemical technology (SVET). Results demonstrate that inclusion of

\* Corresponding author. Tel: +86-057-486325713. Fax: +86-057-486685159.  
E-mail: zhaohaichao@nimte.ac.cn (Haichao Zhao); wangliping@nimte.ac.cn (Liping Wang)

well-dispersed GO-PDA nanosheets leads to the remarkable improvement in the corrosion protection performance of water-borne EP coating.

**Key words:** Water-borne epoxy resin, polydopamine coated graphene oxide, corrosion protection, electrochemical measurement.

### **Introduction**

Severe corrosion of metals has aroused much concern owing to the tremendous economic losses and many potential safety problems. A series of strategies have been proposed to control or delay the corrosion of metals, which include the design of metal substrate, use of corrosion inhibitor, cathodic protection and the coverage of surface coating (organic [1, 2], inorganic [3, 4], and hybrid coatings [5, 6]). Among all of strategies, application of the organic coatings have been the most popular and effective method to protect the metals from corrosion. Among all of organic coatings, epoxy resins have obtained the widespread applications because of their superior chemical inertness, electrical insulating properties and strong adhesion to heterogeneous substrates. However, in present, the epoxy resin commonly used for corrosion protection is the typical solvent-borne system, which contains a certain percentage of volatile compounds (VOCs) that are extremely harmful to environment and human health. Thus, out of the consideration for environments and human health, the use of epoxy resins have to make a shift from solvent-borne system to eco-friendly water-borne system [7, 8]. Incontestable fact is that the long-term corrosion protection performance of the water-borne epoxy coatings are unsatisfactory owing to their inferior barrier property to suppress the penetration of water and corrosive ions

although water-borne epoxy coatings have been commercialized for more than 40 years [8]. Attempts have been extensively done to enhance the corrosion protection performance of the organic coatings by different ways. Many nano-fillers have been studied, i.e. SiO<sub>2</sub> [9, 10], polyaniline (PANI) [11, 12], graphene [13, 14] and hexagonal boron nitride (h-BN) [8, 15].

Recently, graphene, a representative two-dimensional (2D) material, has already attracted more and more attention because of their high thermal conductivity, high electrical conductivity and excellent barrier property [16-18]. However, the complicated fabrication process of water dispersible graphene and the limitation of the corrosion protection of graphene owing to its high electrical conductivity make graphene controversy to act effective additives.

Graphene oxide (GO), a vital derivative of graphene, may be an attractive alternative for graphene owing to the presence of many functional groups (i.e. hydroxyl, carbonyl, carboxyl and epoxy groups) [2, 19]. These groups as active sites make the covalent and/or non-covalent functionalization of GO nanosheets more easily, thus resulting in the improvement of compatibility between the GO nanosheets and solvents/polymers. Furthermore, GO nanosheets can provide a good barrier against the penetration of water, oxygen and corrosive ions, which is attributed to their high surface area [1, 6, 20]. Ramezanzadeh and coworkers revealed that the incorporation of polyisocyanate (PI) resin functionalized GO nanosheets caused the significant improvement in the corrosion protection performance and ionic resistance of the polyurethane (PU) coating [21]. Yang et al. also fabricated the GO nanosheets

with sulfonated aniline trimer (SAT) and the corrosion protection performance of the modified coatings achieves a significant enhancement due to the synergistically enhanced corrosion protection of GO and SAT [2]. Ahmadi and coworkers reported that the silane coating containing silanized graphene oxide has superior corrosion protective performance [5]. However, the corresponding impedance modulus of the sample is extremely low and the long-term corrosion protection performance is not discussed. Therefore, there is still a great challenge to design and develop a facile and efficient synthesis route to disperse GO nanosheets in organic coatings and achieve a long-term corrosion protection.

Dopamine (DA), a hormone and neurotransmitter, can be easily deposited on the surface of a substrate via self-polymerization to form a polydopamine (PDA) layer with excellent adhesion with the any surfaces [22, 23]. Besides, the functional groups (such as catechol, amine, and imine) in DA and PDA can serve as active sites for covalent modification with desired molecules [24, 25]. Lu and coworkers found that polydopamine improve the interfacial interactions between the clay and epoxy resin, leading to the improvement in the thermomechanical properties of epoxy resin [26]. Joon-Hyung Byun et al. also reported that the there was a simultaneous enhancement in mechanical, electrical and thermal properties of graphene oxide paper [19]. Therefore, there are many investigations reported using DA to modify the desired material to achieve enhancement of the dispersion, mechanical and thermal properties [27, 28]. But there is rare investigation about the effect of GO-PDA on the corrosion protection performance of polymers. In this work, we prepared PDA modified GO

nanosheets with a facile and nontoxic method to improve the compatibility of GO with water-borne epoxy coating. The corrosion protection performance of GO-PDA incorporated water-borne epoxy coating was also investigated by electrochemical impedance spectroscopy (EIS) and scanning vibration electrochemical technology (SVET).

## 2.1 Materials

Graphite oxide was purchased from Angxing Technology Co., Ltd. Dopamine hydrochloride and Tris (hydroxymethyl)aminomethane were purchased from Aladdin Industrial Corporation. The ethanol was purchased from Sinopharm Chemical Reagent Beijing Co., Ltd. Epoxy resin (E-51, epoxide number is 0.5, solid content is 98%) and waterborne curing agents (epoxide equivalent is 293, solid content is 60%) were provided by Hangzhou Hanma Paint & Coatings Co., Ltd. Its. The epoxide equivalent and solid content of the curing agent is 293 and 60%,

## 2.2 The modification of GO with PDA

The modification of GO with PDA follows the previous reports [27, 29]. Graphite oxide was first dissolved in 500 mL of Tris-buffer solution (10 mM, pH=8.5) with continuous sonication for 30 min to prepared graphene oxide (GO) aqueous suspensions. Then 800 mg of dopamine hydrochloride was added, and the mixture was stirred vigorously for 24 h at room temperature. After the reaction, the modified GO (GO-PDA) was centrifuged and washed with deionized water and ethanol for several times to remove PDA and other reagents. The GO-PDA mixture was stored for the following experiments. The possible reaction mechanism of the GO-PDA

nanosheets was shown in Fig. 1.

### **2.3. Preparation of epoxy coating**

A certain amount of GO-PDA (33 mg) was dispersed in 1.8 g of ethanol by ultrasonication for 30 min. Then 2 g of waterborne curing agent was added, and the mixture was dispersed homogeneously by ultrasonication for 1 h at the room temperature. Then the epoxy resin (1.3 g) was added into the mixture and stirred for 0.5 h, and the residual solvents were removed by evaporation at 40 °C. The final mixture was fabricated on the Q235 carbon steel electrode by using wire bar coater with a thickness of 20 µm. For comparison, graphite oxide dispersed in ethanol was also used to prepare the epoxy coating according to the above procedure, which was named as GO/EP. Besides, the blank epoxy coating (blank EP) was also prepared for comparison.

### **2.4. Characterization and Measurement**

#### **2.4.1. Characterization**

The morphology of GO and GO-PDA was estimated by transmission electron microscopy (TEM, Tecnai F20, USA) and scanning probe microscopy (SPM Veeco, Dimension 3100, USA). X-ray photoelectronic spectroscopy (XPS, AXIS ULTRA DLD) was utilized to evaluate the chemical structure of the GO and GO-PDA nanosheets. A Fourier transform infrared spectrum (FTIR) was recorded using an FTIR spectrometer (NICOLET 6700, USA) operating at room temperature. Raman spectrum was measured with a confocal Raman spectrometer (Renishaw inVia Reflex, UK) using the wavelength of 532.8 nm. UV-vis spectrum was recorded using a

Lambda 950 UV-vis spectrometer. The crystal structure of the GO and GO-PDA was examined by X-ray diffraction (XRD, D8 ADVANCE, BRUKER, Germany) with a “CuK” radiation source. The fracture surface of the composites was examined by scanning electron microscopy (S4800, Hitachi, Japan).

For contact-angle analysis, the static contact angle was measured by placing a sessile water droplet of 2  $\mu\text{L}$  onto the coating surface using a DCAT21 goniometer.

#### **2.4.2. Electrochemical corrosion studies**

The electrochemical measurements were performed using CHI-660E electrochemical work station. A conventional three-electrode electrochemical system was used, in which a saturated calomel electrode (SCE), a platinum sheet electrode and a specimen (exposed surface area of 1  $\text{cm}^2$ ) were used as reference, counter and working electrodes, respectively. Before each electrochemical measurement, open-circuit potential (OCP) was recorded to reach a steady status. At various time intervals, electrochemical impedance spectroscopy (EIS) was carried out in the frequency range of 100 kHz to 10 mHz with applied 10 mV sinusoidal perturbations. Zview software was used for analyzing the EIS results. All tests were repeated at least three times to ensure reproducibility.

The corrosion protection performance of the coating with artificial scratch that is used to simulate the mechanical damage is also checked by SVET method. The SVET measurement was carried out in 3.5% NaCl solution by a VersaSCAN micro scanning electrochemical workstation (AMETEK, USA). Before the immersion in the 3.5% NaCl solution, an artificial scratch (the length is 2 mm) was made in the coating by a

knife. The vertical current density was recorded on a lattice of  $26 \times 26$  points over an area of  $2.5 \times 2.5 \text{ mm}^2$  (step size  $100 \mu\text{m}$ ). The size of probe tip (Platinum–iridium) was  $10 \mu\text{m}$  and the vibration amplitude was  $30 \mu\text{m}$  with a frequency of  $80 \text{ Hz}$ . All the tests were conducted at the OCP.

### 2.4.3. Analysis of corroded surface

After the long term corrosion, the corroded sample was checked with laser scanning confocal microscope (LSM700, Zeiss), SEM (EVO18, Zeiss) and energy dispersive spectroscopy (EDS).

## 3. Results and Discussion

### 3.1. Characterization of GO-PDA nanosheets

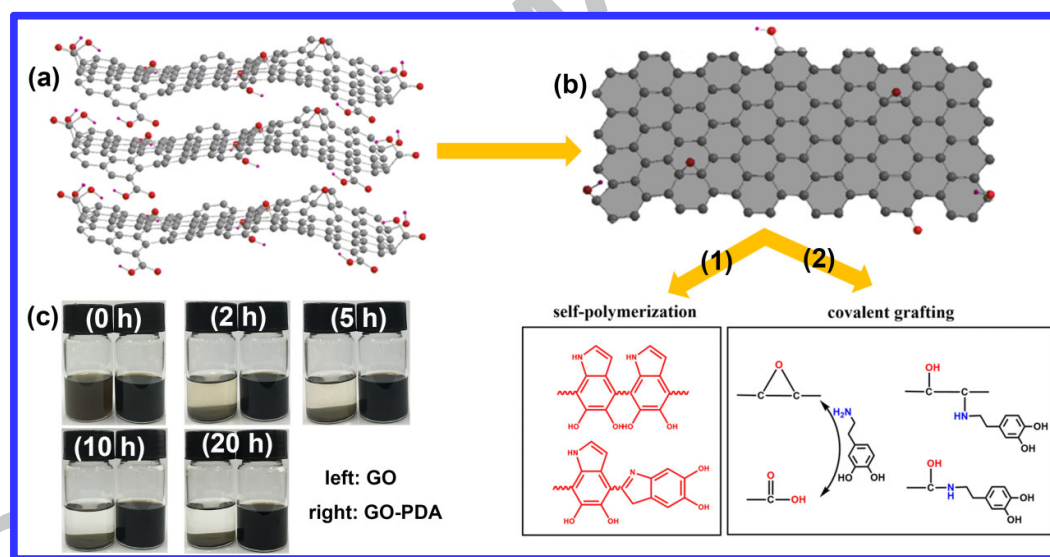


**Fig. 1.** The possible reactions for the modification of GO with PDA. (a) pristine GO, (b) GO-PDA, and (c) the dispersion of GO (left) and GO-PDA (right) in ethanol after various time's storage.

Fig. 1 shows the possible reactions during the modification of GO with PDA. Dopamine is self-polymerized into PDA and absorbs on the surface of GO. In addition,

covalent grafting also exists between the active sites of the GO and DA molecules, promoting the reduction of the GO. The sedimentation test in Fig. 1c presents the dispersing ability of the GO and GO-PDA in ethanol. In this test, the GO and GO-PDA are dispersed in ethanol with ultrasonication for 30 min and then the dispersions are storage without any disturbance for various times. As shown in Fig. 1c, GO has deposited into the bottom of the bottle completely after 5 h of storage while there is no obvious stratification for the GO-PDA/ethanol solution at all the time, indicating that the dispersing ability of the GO in ethanol is significantly improved after the modification with PDA.

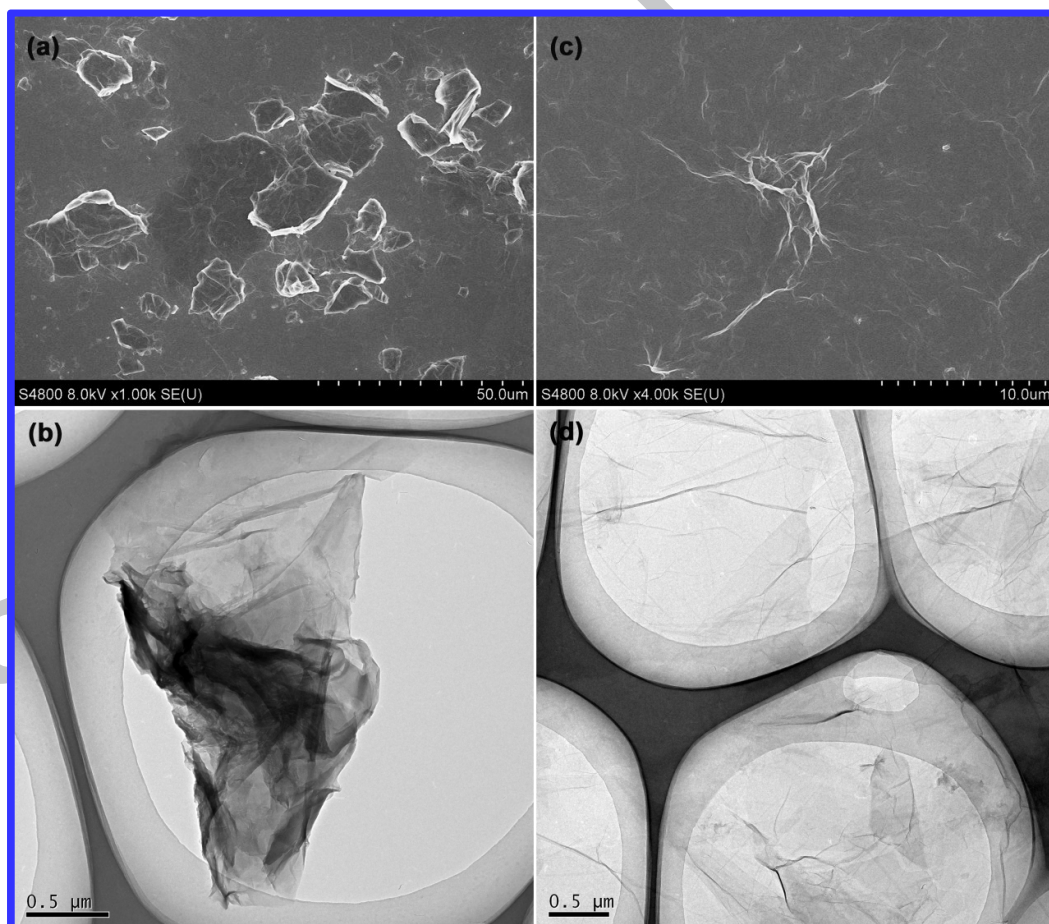


**Fig. 2.** SEM and TEM morphologies of (a-b) GO and (c-d) GO-PDA dispersed in

ethanol.

The morphologies of GO and GO-PDA dispersed in ethanol are checked by SEM and TEM, as shown in Fig. 2. The GO nanosheets dispersed in ethanol at the Si substrate and Cu grid exist mostly in the relative thick layers, which is attributed to the poor dispersion of GO nanosheets (Fig. 2a-b). After the modification with PDA, the GO-PDA nanosheets are well dispersed in ethanol, and exist in thin and transparent nanosheets with several layers and large surface area (Fig. 2c-d). The surface morphologies and the thickness of GO and GO-PDA are further examined by SPM. As shown in Fig. 3a, the GO mostly exists in the relative thick layers and the thickness of the GO layers reaches about 25~38 nm. According to the previous report, the thickness of GO with a single layer is ~0.9 nm while the average thickness of GO-PDA nanosheet with a single layer is 2~3 nm, indicating that the increase in thickness of 1.1~2.1 nm is due to the presence of poly(dopamine) on the GO nanosheets (Fig. 3b) [24, 30]. Also, it can be observed from Fig. S1 that GO exhibits a sharp peak centered at  $2\theta=9.1^\circ$ , which is similar to the previous report [31]. For GO-PDA, the sharp diffraction peak for GO becomes weak and shifts to lower degree ( $2\theta=6.9^\circ$ ), which indicates that the interlayer spacing between the GO layers increases. This is because PDA can absorb on the surface of GO nanosheets or the chemical bonding exists between GO and PDA. Thus, it can be inferred from the increased thickness that the GO surface is modified with PDA successfully.

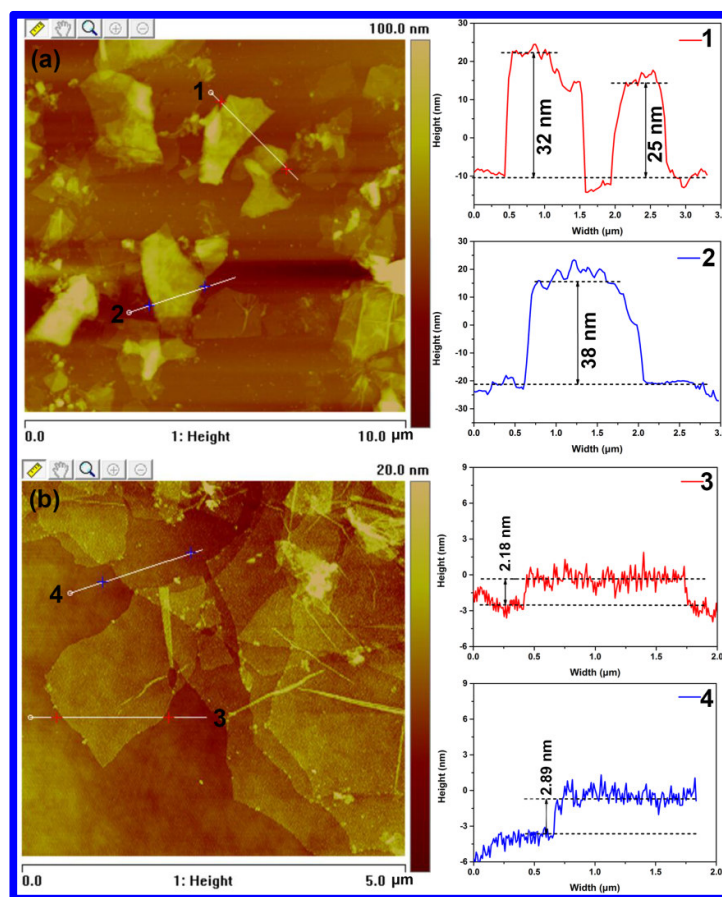


**Fig. 3.** SPM images and corresponding height profiles of (a) GO and (b) GO-PDA.

Identification of GO modified with PDA is also examined by FTIR as shown in Fig. 4a. The characteristic peaks of GO are identified as follows: O-H at  $3399\text{ cm}^{-1}$ , carboxy C=O at  $1734\text{ cm}^{-1}$ , aromatic C=C at  $1624\text{ cm}^{-1}$ , C-OH stretching vibrations at  $1211\text{ cm}^{-1}$  and C-O stretching at  $1054\text{ cm}^{-1}$  [32, 33]. After modification with PDA, the peak of C=O stretching vibrations at  $1735\text{ cm}^{-1}$  decreases largely owing to the reduction of GO by PDA. Two new peaks appear at  $1385\text{ cm}^{-1}$  and  $1504\text{ cm}^{-1}$ , which are assigned to the C-N framework vibration and N-H stretching vibration, respectively, indicating the reaction between the epoxide group and the amine group [19, 34].

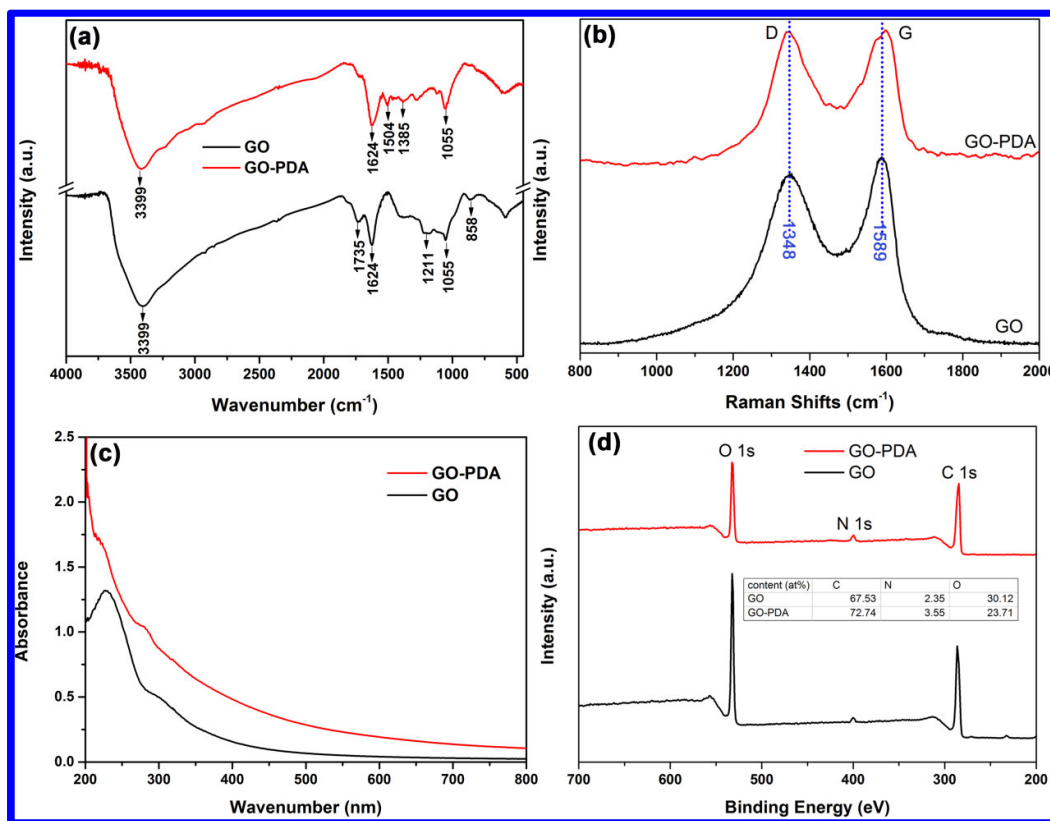


**Fig. 4.** (a) FT-IR spectra of GO and GO-PDA, (b) Raman spectra of GO and GO-PDA, (c) UV-vis spectra of GO and GO-PDA (the solvent is ethanol), (d) XPS survey spectra of GO and GO-PDA.

Raman spectroscopy is employed to distinguish the ordered and disordered carbon structures. It can be seen from Fig. 4b that GO exhibits the G band at  $1589\text{ cm}^{-1}$  and D band at  $1348\text{ cm}^{-1}$ , respectively [35]. After modification with PDA, the G band becomes broadened and shifts from  $1589\text{ cm}^{-1}$  (graphite) to  $1598\text{ cm}^{-1}$ , which is ascribed to plane vibration of  $sp^2$  carbon atoms, indicating the successful modification of PDA [24]. The  $I_D/I_G$  ratio present a slight increase from 0.9 for GO to 0.93 for GO-PDA, indicating that no more defects are introduced after the modification of GO with PDA and the GO preserves its basic structural properties [34, 36].

The variation of the UV-vis absorption spectroscopy of GO and GO-PDA is also

checked as shown in Fig. 4c. For the UV-vis spectra of GO, a characteristic absorption peak at 228 nm and a shoulder peak at about 285~320 nm can be observed, which is attribute to the  $\pi \rightarrow \pi^*$  transition of aromatic C=C bonds and  $n \rightarrow \pi^*$  transition of the carbonyl groups, respectively [24, 35, 37]. After modification with PDA, GO is partially reduced to graphene by dopamine. Besides, a new peak appears at 282 nm, which is a typical absorption of catechols in polydopamine, and similar behaviors are also reported in the previous investigation [22, 37]. Furthermore, the color of the GO suspension varies from brown to black after modification with of PDA, suggesting the reduction of GO [37].

In addition, the variation on content of various elements and the chemical bonds of GO and GO-PDA are also examined by XPS as shown in Fig. 4d and Fig. 5. Both GO and GO-PDA showed similar peaks of C 1s, O 1s and N 1s in the full XPS spectra (Fig. 4d). The N element in GO may be originated from the preparation process of GO. But the content of N for GO-PDA increases by 1.2 at.% with respect to that of GO. C 1s XPS spectrum of GO can be curved into four peaks with binding energies at 284.6, 286.7, 287.3 and 288.6 eV, which correspond to the C=C, C-O, C=O, and O-O-C=O components, respectively [38]. In contrast with GO, a new strong peak at 285.5 eV assigned to the C-N bond appears in the GO-PDA, which can be another fingerprint for formation of PDA [24, 32].

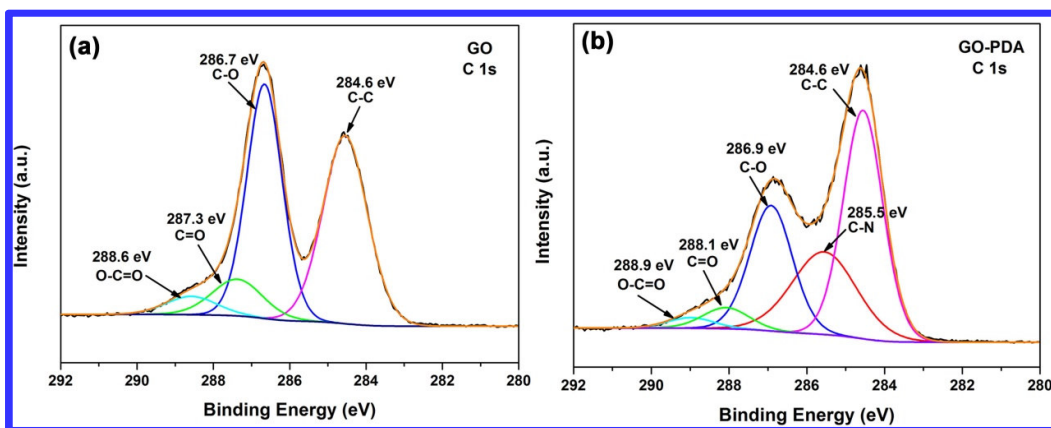
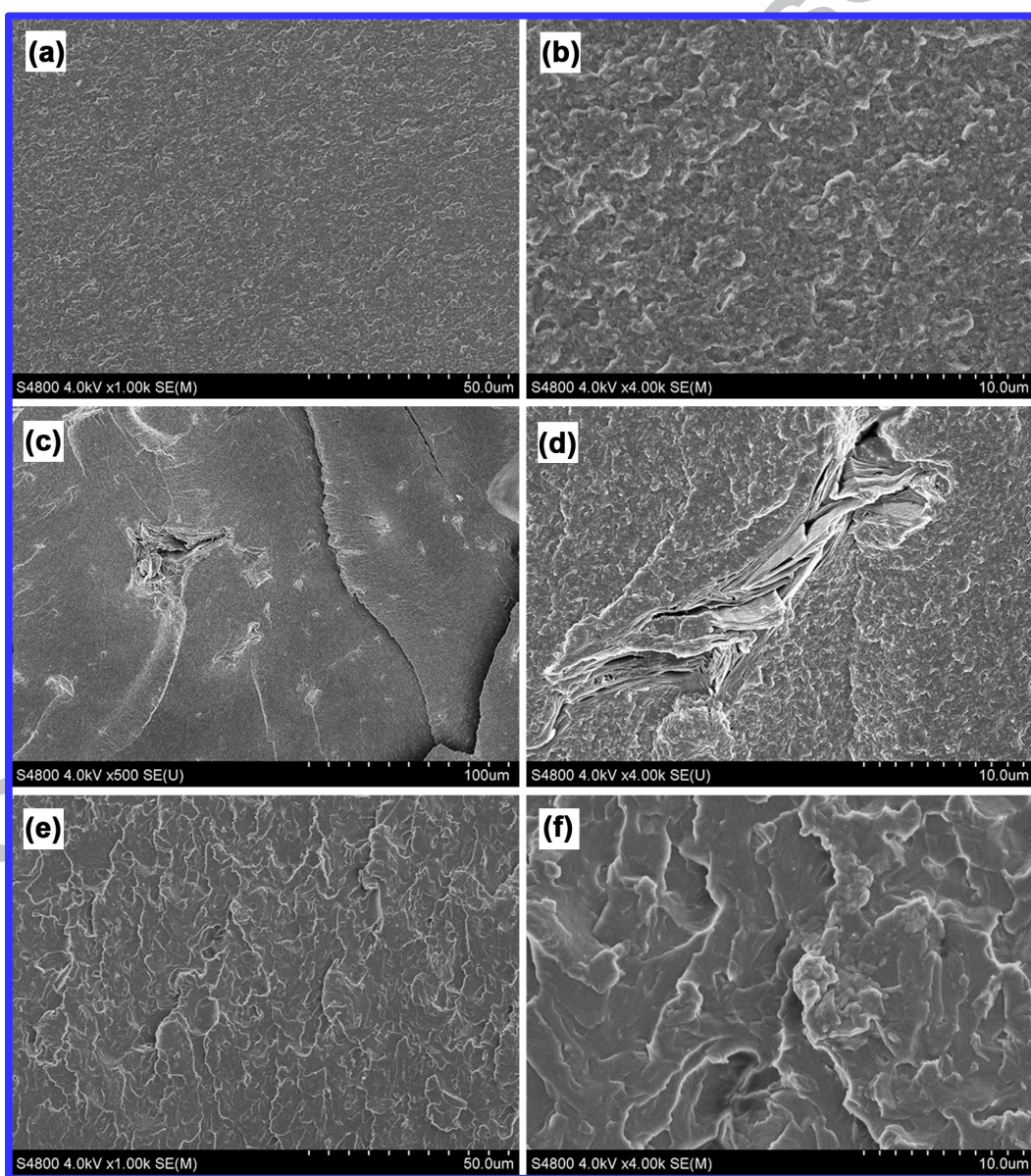


Fig. 5. XPS spectra of C1s for (a) GO and (b) GO-PDA.



**Fig. 6.** The SEM morphologies of fracture surfaces of (a-b) blank EP, (c-d) GO/EP and (e-f) GO-PDA/EP.

Fig. 6 displays the SEM morphologies of fracture surfaces of the samples. As observed in Fig. 6a-b, the blank EP shows a very clean and smooth fracture surface while the fracture surface of blank EP is loose and porous. When GO is dispersed in EP matrix, some aggregation and defects appear at the fracture surface, implying the poor dispersion performance of GO in EP (Fig. 6c-d). In case of the GO-PDA/EP, GO-PDA has a well compatibility with EP matrix and the fracture surface becomes denser than blank EP and GO/EP (Fig. 6e-f). Further to our purpose, modification of GO with PDA achieves a homogeneous dispersion and compatibility in ethanol and EP without destroying the sheet structures of GO. This achievement will provide a novel technology for preparing epoxy coating with excellent barrier effect on corrosion protection.

### 3.2. Corrosion protection performance of GO-PDA/EP coatings

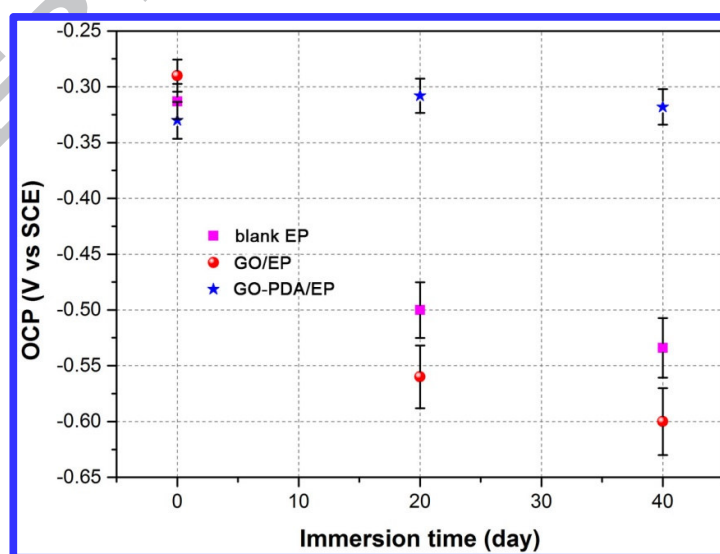


**Fig. 7.** The variation on OCP value for different coating/steel systems under 3.5%

NaCl solution.

The OCPs of coating/steel systems have been recorded at various time intervals under 3.5% NaCl solution as presented in Fig. 7. The OCPs of blank EP and GO/EP have shifted to a negative value with increasing immersion time owing to the penetration of water in EP matrix, and the OCP of GO/EP (from -0.29 to -0.6 V) is more negative than that of blank EP (from -0.31 to -0.53 V). This is attributed to the fact that the poor dispersion of GO nanosheets in EP causes more defects and pores in EP matrix, thus leading to the negative OCP. Interestingly, it is noteworthy that the GO-PDA/EP coating exhibits more positive OCP value ( $\sim -0.32$  V) and there is no obvious variation on OCP value of GO-PDA/EP because the homogeneous incorporation of GO-PDA in EP matrix significantly enhances the coating's compactness and hence inhibits the penetration of corrosive medium. Besides, the improved water contact angle (the water contact angle is  $66^\circ$ ,  $65^\circ$  and  $73^\circ$  for the blank EP, GO/EP and GO-PDA/EP, respectively) after the addition of GO-PDA is also beneficial to the enhanced anticorrosion property of epoxy (Fig. S2).

EIS was employed to evaluate and compare the barrier and corrosion protection performance of composite coatings under 3.5% NaCl solution at various time intervals. The Nyquist and Bode plots of different coating/steel systems are shown in Figs. 8. According to Fig. 8a and 8b, a broad relaxation time can be observed in the Nyquist and Bode phase plot for all coating/steel systems after 0.5 h immersion. Even if it is seen as one time constant, there are more than one and their time constants overlap enough to hide out true nature of the system. Diffusion is the one and other

processes and physical parts like double layer capacitance or even more as distribution of the coating capacitance (depending on lateral and epitaxial) are the source of overlapping without the ability to discern them as more than one time constant. The equivalent circuit in Fig. 9a is used to fit the EIS results which contains the solution resistance ( $R_s$ ), the coating constant phase element ( $CPE_c$ ) and the pore resistance ( $R_p$ ), the double layer constant phase element ( $CPE_{dl}$ ) and the charge transfer resistance ( $R_{ct}$ ). The constant phase element (CPE) is employed instead of the ideal capacitance (C) because of the “scattering effect” resulting from the heterogeneity of the coating surface [39, 40]. And the blank EP coated steel electrode exhibits largest capacitive loop and highest impedance modulus ( $2.04 \times 10^8 \Omega \text{ cm}^2$ ) compared to those of GO/EP ( $1.10 \times 10^8 \Omega \text{ cm}^2$ ) and GO-PDA/EP ( $1.16 \times 10^8 \Omega \text{ cm}^2$ ) coated steel electrodes after 0.5 h immersion (Fig. 8a and 8b). As the immersion time is up to 20 days, the barrier performance for all coatings decreases owing to the absorption of corrosive medium and the creation of transport pathways to the steel substrate through the defects or pores. It can be observed that a new diffusion field at the low frequencies appears around the blank EP and GO-PDA/EP coated steel electrode, respectively (Fig. 8c and 8d). At this moment, Warburg impedance element ( $Z_w$ ) is included in the equivalent circuit (Fig. 9b) since the diffusion effect in the coating or the coating-substrate interface dominates corrosion at low frequencies for the blank EP and GO-PDA/EP coated steel electrode. For the GO/EP coated steel electrode, the second time constant at the low frequencies becomes obviously owing to the acceleration of the corrosion induced charge transfer between at the metal

substrate/coating interfaces (Fig. 8c and 8d), thus the equivalent circuit in Fig. 9a is still appropriate. Different from the EIS results after 0.5 h immersion, the GO-PDA/EP coating exhibits the superior protective performance than blank EP and GO/EP coating owing to the barrier effect from the homogeneous dispersion of GO-PDA in EP matrix and the impedance modulus is about  $2.46 \times 10^7 \Omega \text{ cm}^2$ . Therefore, it is inferred that the diffusion process in GO-PDA/EP coated steel electrode corresponds to the diffusion of corrosive medium in the coating. Descending trend is again seen with increasing the immersion time to 40 days (Fig. 8e and 8f). In this stage, the corrosion is further accelerated because of the diffusion of the corrosive medium in the coating or coating-substrate interface.

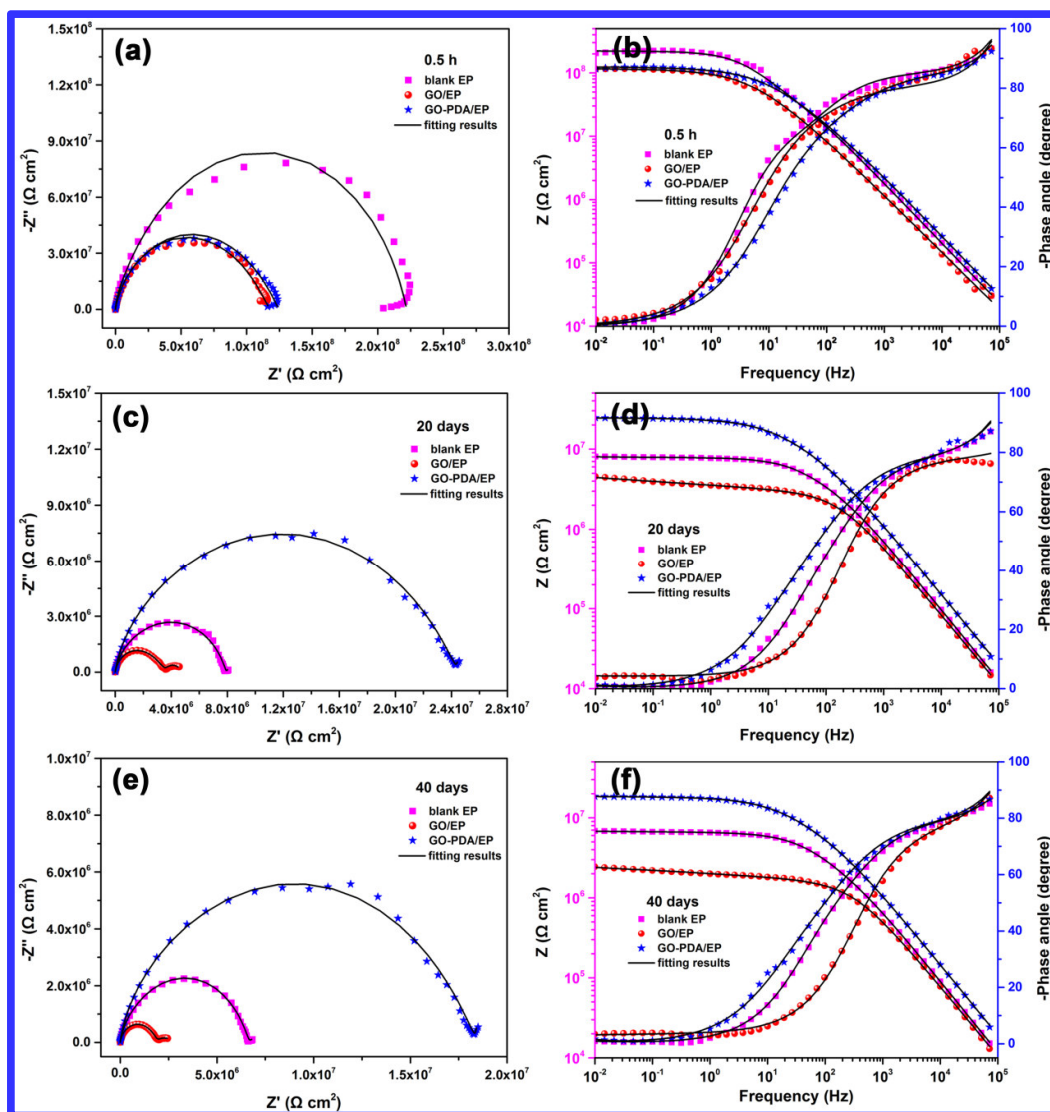


**Fig. 8.** EIS plots of different coating/steel systems under 3.5% NaCl solution at various time intervals, (a) 0.5 h, (b) 20 days and (c) 40 days. Scatters are experimental data and black lines are fitting results.

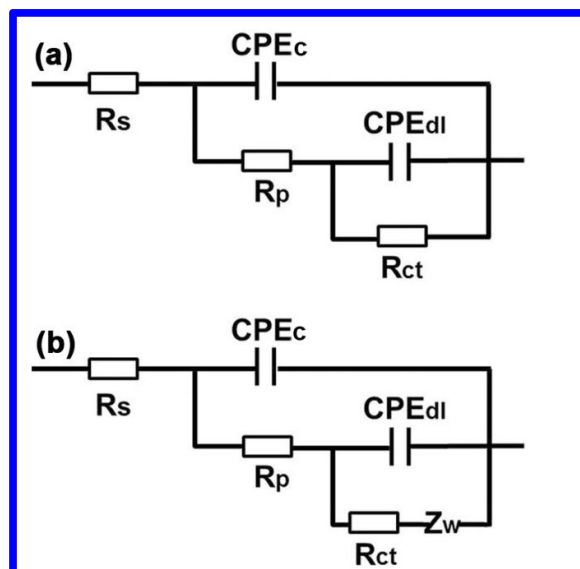


**Fig. 9.** The proposed equivalent circuit model for fitting (a) all EIS results at 0.5 h days immersion and the EIS results of GO/EP at 20 and 40 days immersion; (b) EIS results of blank EP and GO-PDA/EP at 20 and 40 days immersion.

To simplify the analysis of EIS plots, the impedance modulus ( $Z$ ) at the lowest frequency (10 mHz) is employed to directly evaluate the corrosion performance of the samples. It can be obviously seen from Fig. 10a that the incorporation of GO into the EP matrix causes the most pronounced decrease of  $Z$  compared to the blank EP sample with increase in immersion time. The possible reason is that the poor dispersion of GO in EP produces more defects or pores in the coating (see Fig. 6c-d), thus leading to the quick transportation of corrosive medium from coating to substrate and the corrosion of substrate. In case of the GO-PDA/EP, the stable dispersion of GO-PDA in EP makes denser cross-sectional structure compared to the GO/EP and blank EP sample, thus the GO-PDA/EP coating exhibits excellent corrosion protection performance.

In addition, breakpoint frequency ( $f_b$ ), the frequency at  $-45^\circ$  phase angle, can be

used to evaluate the microscopic delaminated areas between the coating and substrate [21, 41]. When the corrosive medium diffuses to the coating-substrate interface, the anodic reaction induces the corrosion of metal surface ( $\text{Fe} \rightarrow \text{Fe}^{2+} + 2\text{e}^-$ ) and cathodic reaction causes the creation of hydroxyl ions ( $1/2\text{O}_2 + \text{H}_2\text{O} + 2\text{e}^- \rightarrow 2\text{OH}^-$ ) at the coating/metal interface, thus resulting in the development of corrosion products beneath the coating. The accumulation of the corrosion products in long-term would lead to the coating delamination from the substrate surface at some regions and the decline of the coating protection performance. From Fig. 10b, it can be seen that the  $f_b$  shifts from low frequencies to higher frequencies with prolonged immersion time. The shift of  $f_b$  is the most pronounced for the GO/EP sample (7.89~420 Hz), which implies that incorporation of GO cannot enhance the barrier property of the EP but weaken the protection performance owing to the introduction of defects caused by the poor dispersion of GO. The  $f_b$  of blank EP coating shifts from 5.39 to 106.5 Hz. In case of the GO-PDA/EP (16~65.8 Hz), the  $f_b$  is lower than other samples, indicating that the less corrosion and coating delamination of the substrate surface. Therefore, well dispersion of GO is critical for the improving the protection performance of EP matrix.

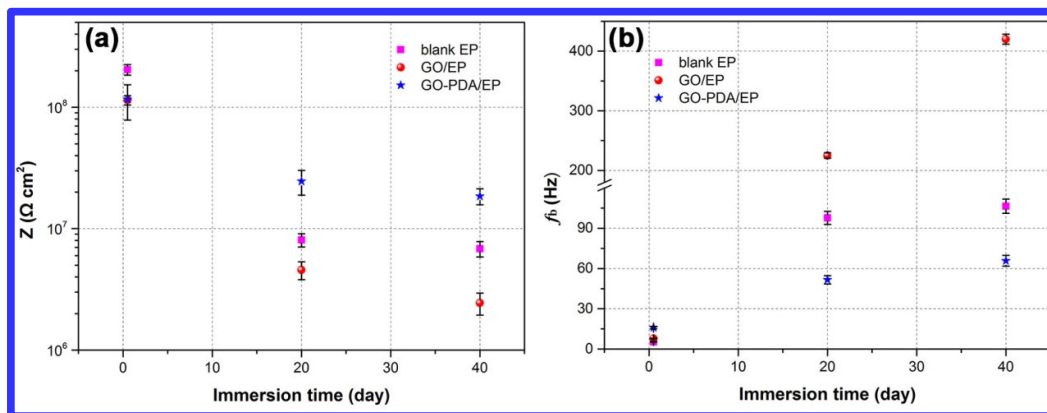


**Fig. 10.** The variation of (a)  $Z$  and (b)  $f_b$  for different coating/steel systems after immersion in 3.5% NaCl solution at various time intervals.

The EIS results are further analyzed by fitting with equivalent circuits in Fig. 9 and all the experimental EIS results are fitted well with appropriate equivalent circuits (the black lines in Fig. 8). The variation of the electrical parameters ( $R_p$ ,  $R_{ct}$ ,  $CPE_c$  and  $CPE_{dl}$ ) obtained from fitting process is presented in Fig. 11.  $R_p$ , the electric resistance of coating against transfer of ions through pores of coating, can be used to measure the coating porosity and degradation.  $CPE_c$  is related to the water barrier property of the organic coatings, which will increase during the immersion because of the absorption of water with higher dielectric constant ( $\sim 80$ ) [40, 42]. It can be observed from Fig. 11a that the  $R_p$  values decrease with increasing immersion time for all coating systems. The decrease of  $R_p$  value for blank EP and GO/EP is more pronounced than GO-PDA/EP coating. Similar trends can also be found for the  $CPE_c$  (Fig. 11c), but with the opposed direction to  $R_p$ . The higher  $R_p$  and lower  $CPE_c$  clearly show that the incorporation of well dispersed GO-PDA can improve the coating's barrier property against the water permeation.  $CPE_{dl}$  and  $R_{ct}$  are directly related to the corrosion performance of the coating. It can be found that the evolution of  $CPE_{dl}$  and

$R_{ct}$  is similar with the  $CPE_c$  and  $R_p$ . The lower  $CPE_{dl}$  and higher  $R_{ct}$  values of GO-PDA/EP, compared to the blank EP and GO/EP (see Fig. 11b and 11d), suggest that the incorporation of GO-PDA can efficiently inhibit the penetration of corrosive medium to the coating/metal interface, which can be attributed to the excellent barrier effect of homogeneous GO-PDA in EP matrix.

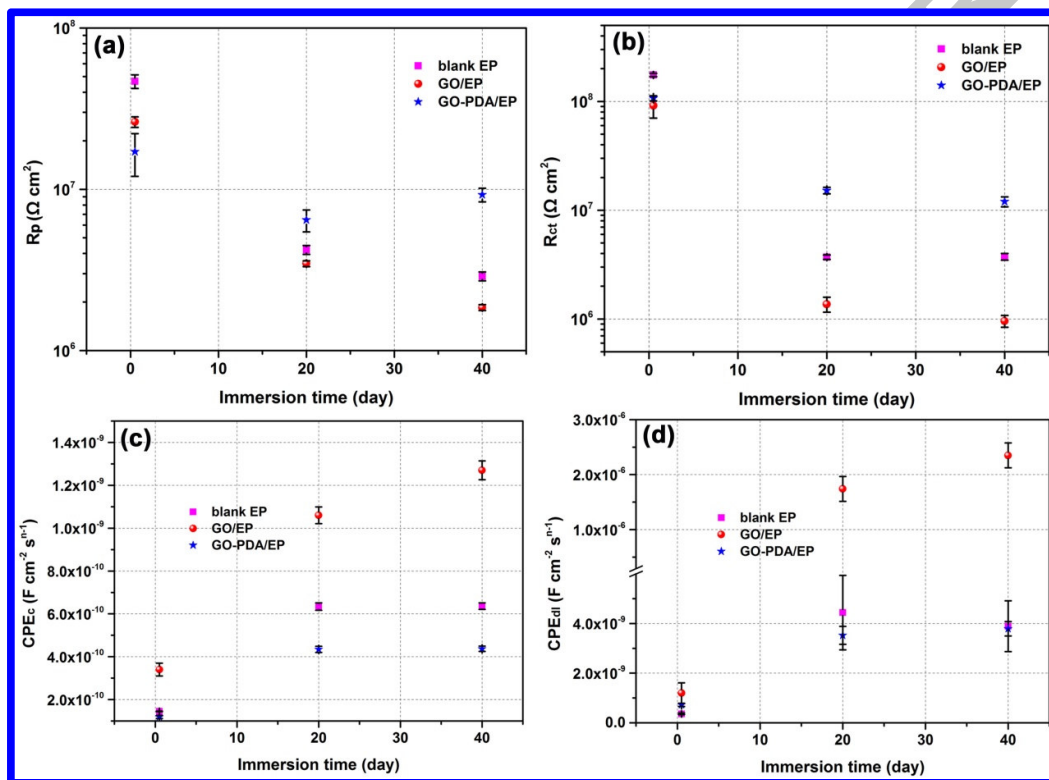


**Fig. 11.** Variation of the electrical parameters (a)  $R_p$ , (b)  $R_{ct}$ , (c)  $CPE_c$  and (d)  $CPE_{dl}$  derived from EIS data for different coating/steel systems during the immersion in 3.5% NaCl solution.

Based on the analysis above, it can be inferred that GO-PDA/EP coating exhibits more superior corrosion protection performance than blank EP and GO/EP. Further, in order to investigate the corrosion process at metal/coating interface, the coating is detached from the substrate surface after 40 days immersion in 3.5 % NaCl solution.

Fig. 12 shows the macro and micro morphologies of the substrate surface after removal of blank EP, GO/EP and GO-PDA/EP. From the perspective of macro morphologies, there are some black areas with pit corrosion and corrosion products on the substrate surface coated with blank EP and GO/EP (Fig. 12a and 12d) while there are less pit corrosion and corrosion products on the substrate surface coated with GO-PDA/EP (Fig. 12g). To better observe the micro morphologies of the substrate surface, SEM was employed. As shown in Fig. 12b, 12c and 12f, the substrate surface of blank EP and GO/EP is rough and covered with corrosion products and cavities. Besides, many white matters are observed in the un-corroded region of the substrate surface for blank EP and GO/EP (Fig. 12f). The substrate surface of GO-PDA/EP presents more uniform surface with obvious scratches owing to the polish, and there is no obvious accumulation of corrosion products. To analysis the variation of the elements at the substrate surface, we choose five different regions (marked in Fig. 12) from the samples to make an EDS analysis.

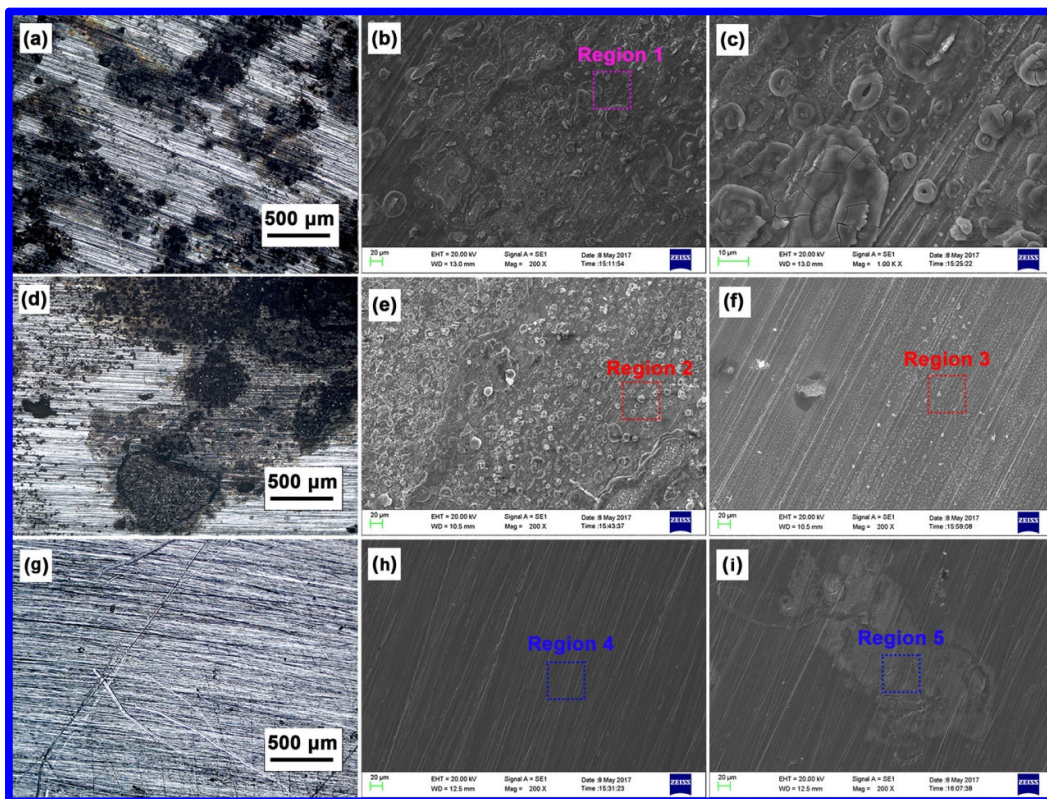


**Fig. 12.** LSCM and SEM morphologies of substrate surface after 40 days immersion in 3.5% NaCl solution: (a-c) blank EP, (d-f) GO/EP and (g-i) GO-PDA/EP. (The marked region is used for the EDS analysis)

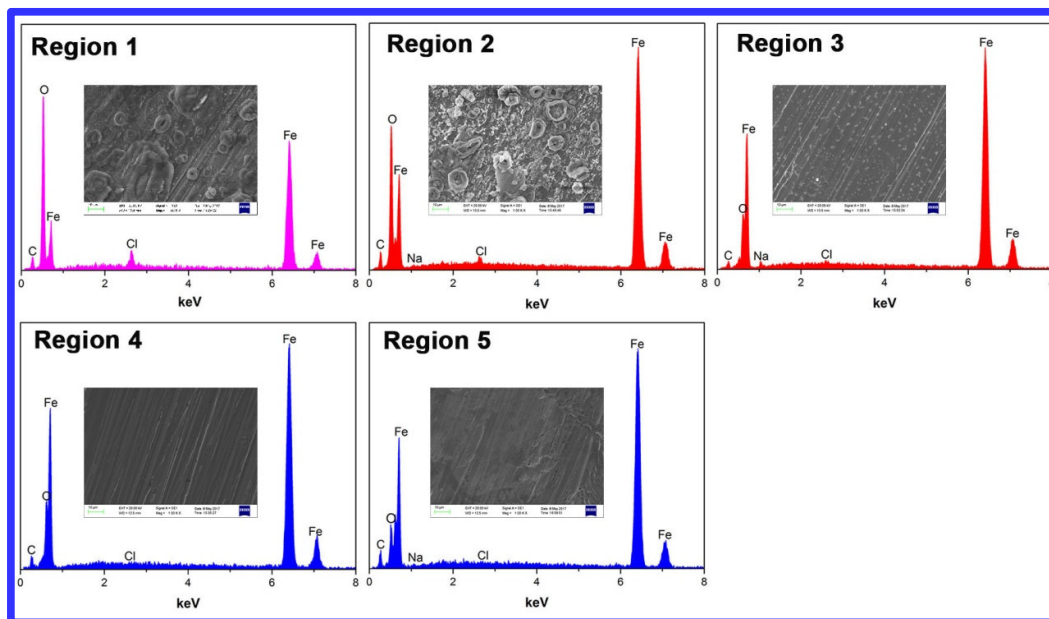


**Fig. 13.** The EDS results of five regions for blank EP (Region 1), GO/EP (Region 2-3) and GO-PDA/EP (Region 4-5).

As shown in Fig. 13, the corroded substrate surface of blank EP (Region 1) is mainly composed of Fe (51.47%), O (37.94%), C (8.97%) and Cl (1.61%), indicating that many water and corrosive ions has reached the substrate surface. For the GO/EP, the contents of O (24.44%) and Cl (0.68%) for the corroded substrate surface (Region 2) are much lower compared to those of blank EP. In case of the un-corroded substrate surface (Region 3), the content of O is only about 1.66% and it is proved that the white matter in Fig. 12f is assigned to NaCl owing to the significant improvement of the content of Na (1.43%). In case of the GO-PDA/EP, the content of O and Cl for the substrate surface (Region 4) is 1.52% and 0.1%, respectively. As for the substrate surface with less corrosion (Region 5), the content of O and Cl for the substrate surface is 9.2% and 0.02%, respectively. Based on the variation of the content of elements, it can be found that the region with less corrosion has less content of O and

Cl, which is mainly attributed to the excellent barrier property of EP by adding GO-PDA nanosheets.

**Table 1** Variation of the content for different elements.

Elements (wt %)	Fe	C	O	Cl	Na
<b>Region 1</b>	51.47	8.97	37.94	1.61	--
<b>Region 2</b>	64.84	9.73	24.44	0.68	0.31
<b>Region 3</b>	90.78	5.88	1.66	0.26	1.43
<b>Region 4</b>	89.54	8.83	1.52	0.1	--
<b>Region 5</b>	79.16	11.21	9.2	0.02	0.42

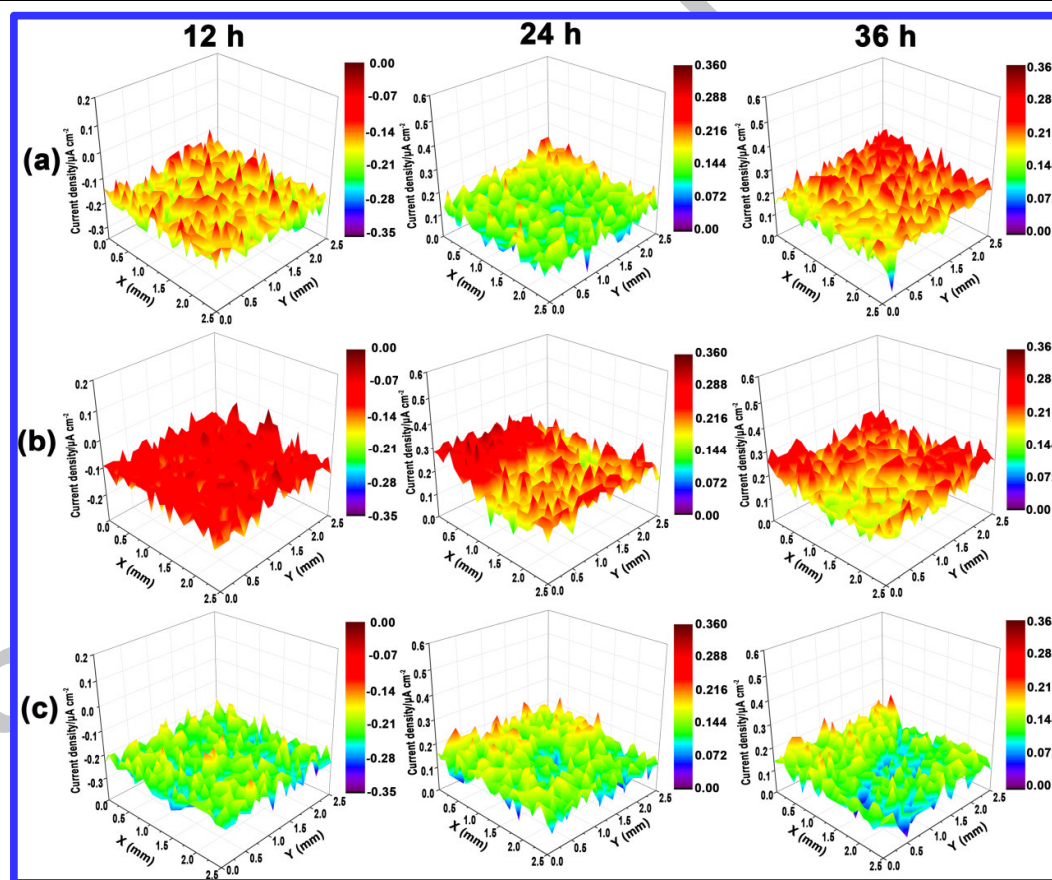


**Fig. 14.** SVET maps of the current density for the defected surface of (a) blank EP, (b) GO/EP and (c) GO-PDA/EP after various immersion time in 3.5% NaCl solution.

The artificial defect (around 2 mm length and deep to the Q235 carbon steel surface) is scratched carefully on the coatings by a knife and exposed in 3.5% NaCl solution. The variation of the potential signals around artificial defects is recorded and then transformed into the current density, as shown in Fig. 14. For blank EP (Fig. 14a), the noticeable cathodic current density is measured after 12 h of immersion and the region of cathodic current density for blank EP is  $-0.3 \sim -0.1 \mu\text{A cm}^{-2}$ , suggesting that cathodic reaction is active during this immersion time. With increasing immersion time (24 to 36 h), anodic dissolution occurs for the carbon steel close to scratch and the highest anodic current density in the scan region varies from  $0.25 \mu\text{A cm}^{-2}$  (24 h) to  $0.3 \mu\text{A cm}^{-2}$  (36 h). More obviously, the area of scan region with the high anodic current density increases with increasing immersion time, indicating the aggravation of the corrosion for the substrate. In Fig. 14b, cathodic reaction is also dominated for GO/EP during 12 h of immersion. The area with the high anodic current density at 24 h and 36 h is much more than that of blank EP and the highest anodic current density is about  $0.35 \mu\text{A cm}^{-2}$ , which is due to the water penetration from the scratch and the defects caused by the agglomerated GO. Although the GO-PDA/EP has similar behavior with blank EP and GO/EP, its highest anodic current density ( $0.24 \mu\text{A cm}^{-2}$  at 24 and 36 h) and the area with the high anodic current density is lower and less than blank EP and GO/EP (Fig. 14c). This indicates that GO-PDA/EP with mechanical damages can also play a better protected role than blank EP.

Based on the above results, we can infer that the corrosion protection performance of EP matrix can be improved by incorporating GO-PDA nanosheets and

the corresponding corrosion protection mechanism is shown in Fig. 15. For the blank EP, the corrosive medium and  $O_2$  diffuse along the defects and pores in the coating, and the corrosion of the substrate happens when the corrosive medium reaches to the coating/substrate interface. In case of the GO-PDA/EP, the enhancement of corrosion protection performance can be attributed to the following reasons: (1) the well-dispersed GO-PDA nanosheets make the EP matrix denser, and there is less defects and pores in the coating, inhibiting the diffusion of corrosive medium. (2) the incorporated GO-PDA nanosheets with a higher aspect ratio provides an improved water repellent property and excellent barrier layer to preeminently block diffusive paths for electrolyte permeation, thus protecting the underlying substrate from corrosion attack.

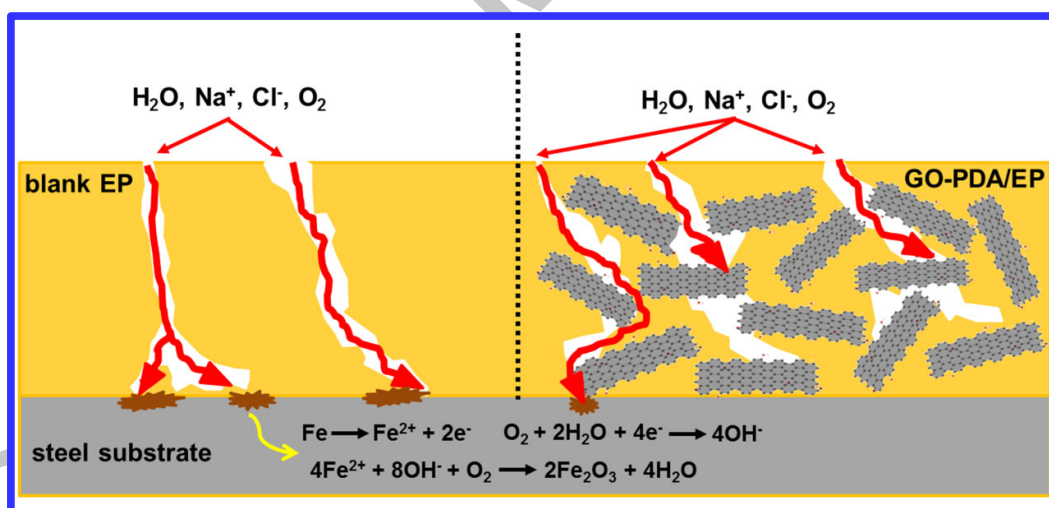


**Fig. 15.** Corrosion protection mechanism of GO-PDA/EP.

#### 4. Conclusions

In summary, we reported an eco-friendly anticorrosive water-borne epoxy coating incorporated with the dopamine functionalized GO nanosheets. The successful modification of GO nanosheets with PDA could be confirmed by TEM,

SPM, FT-IR, Raman, UV and XPS. Besides, the GO-PDA nanosheets had well dispersion in the ethanol and superior compatibility with waterborne epoxy matrix. Long-term electrochemical results showed that the corrosion protection performance of GO-PDA/EP was improved remarkably with respect to the blank EP and GO/EP owing to the strong interfacial bonding between GO-PDA and EP matrix as well as reinforced barrier property originated from GO-PDA. Furthermore, it could be found from the LSCM, SEM and corresponding EDS results that the substrate surface had been corroded severely and the content of oxygen increased dramatically owing to the penetration of corrosive medium whereas there was less corrosion region at the substrate surface coated with GO-PDA/EP, which further demonstrated the excellent corrosion protection and barrier properties of the GO-PDA/EP. More importantly, the GO-PDA/EP with mechanical damages still exhibits better corrosion protection performance than blank EP.

### **Acknowledgements**

The authors gratefully acknowledged financial support provided by the Strategic Priority Research Program of the Chinese Academy of Sciences (XDA13040601), the National Key Basic Research Program (No.2014CB643302) and “One Hundred Talented People” of the Chinese Academy of Sciences (Y60707WR04).

**References**

- [1] B. Ramezanzadeh, A. Ahmadi, M. Mahdavian, Enhancement of the corrosion protection performance and cathodic delamination resistance of epoxy coating through treatment of steel substrate by a novel nanometric sol-gel based silane composite film filled with functionalized graphene oxide nanosheets, *Corrosion Science* 109 (2016) 182-205.
- [2] H. Lu, S. Zhang, W. Li, Y. Cui, T. Yang, Synthesis of Graphene Oxide-Based Sulfonated Oligoanilines Coatings for Synergistically Enhanced Corrosion Protection in 3.5% NaCl Solution, *ACS applied materials & interfaces* 9(4) (2017) 4034-4043.
- [3] M. Cui, J. Pu, J. Liang, L. Wang, G. Zhang, Q. Xue, Corrosion and tribocorrosion performance of multilayer diamond-like carbon film in NaCl solution, *RSC Adv.* 5 (2015) 104829-104840.
- [4] M. Cui, J. Pu, G. Zhang, L. Wang, Q. Xue, The corrosion behaviors of multilayer diamond-like carbon coatings: influence of deposition periods and corrosive medium, *RSC Adv.* 6(34) (2016) 28570-28578.
- [5] A. Ahmadi, B. Ramezanzadeh, M. Mahdavian, Hybrid silane coating reinforced with silanized graphene oxide nanosheets with improved corrosion protective performance, *RSC Adv.* 6(59) (2016) 54102-54112.
- [6] B. Ramezanzadeh, Z. Haeri, M. Ramezanzadeh, A facile route of making silica nanoparticles-covered graphene oxide nanohybrids (SiO<sub>2</sub>-GO); fabrication of SiO<sub>2</sub>-GO/epoxy composite coating with superior barrier and corrosion protection performance, *Chemical Engineering Journal* 303 (2016) 511-528.

- [7] F. Chen, P. Liu, Conducting Polyaniline Nanoparticles and Their Dispersion for Waterborne Corrosion Protection Coatings, *ACS applied materials & interfaces* 3 (2011) 2694-2702.
- [8] M. Cui, S. Ren, J. Chen, S. Liu, G. Zhang, H. Zhao, L. Wang, Q. Xue, Anticorrosive performance of waterborne epoxy coatings containing water-dispersible hexagonal boron nitride (h-BN) nanosheets, *Applied Surface Science* 397 (2017) 77-86.
- [9] M. Conradi, A. Kocijan, D. Kek-Merl, M. Zorko, I. Verpoest, Mechanical and anticorrosion properties of nanosilica-filled epoxy-resin composite coatings, *Applied Surface Science* 292 (2014) 432-437.
- [10] T. Simovich, A.H. Wu, R.N. Lamb, Hierarchically rough, mechanically durable and superhydrophobic epoxy coatings through rapid evaporation spray method, *Thin Solid Films* 589 (2015) 472-478.
- [11] C.-J. Weng, C.-H. Chang, C.-W. Peng, S.-W. Chen, J.-M. Yeh, C.-L. Hsu, Y. Wei, Advanced Anticorrosive Coatings Prepared from the Mimicked Xanthosoma Sagittifolium-leaf-like Electroactive Epoxy with Synergistic Effects of Superhydrophobicity and Redox Catalytic Capability, *Chemistry of materials* 23 (2011) 2075-2083.
- [12] X.-Z. Gao, H.-J. Liu, F. Cheng, Y. Chen, Thermoresponsive polyaniline nanoparticles: Preparation, characterization, and their potential application in waterborne anticorrosion coatings, *Chemical Engineering Journal* 283 (2016) 682-691.

[13] Z. Yang, W. Sun, L. Wang, S. Li, T. Zhu, G. Liu, Liquid-phase exfoliated fluorographene as a two dimensional coating filler for enhanced corrosion protection performance, *Corrosion Science* 103 (2016 ) 312–318.

[14] C. Chen, S. Qiu, M. Cui, S. Qin, G. Yan, H. Zhao, L. Wang, Q. Xue, Achieving high performance corrosion and wear resistant epoxy coatings via incorporation of noncovalent functionalized graphene, *Carbon* 114 (2017) 356-366.

[15] E. Husain, T.N. Narayanan, J.J. Taha-Tijerina, S. Vinod, R. Vajtai, P.M. Ajayan, Marine Corrosion Protective Coatings of Hexagonal Boron Nitride Thin Films on Stainless Steel, *ACS applied materials & interfaces* 5 (2013) 4129–4135.

[16] C. Mattevi, G. Eda, S. Agnoli, S. Miller, K.A. Mkhoyan, O. Celik, D. Mastrogiovanni, G. Granozzi, E. Garfunkel, M. Chhowalla, Evolution of Electrical, Chemical, and Structural Properties of Transparent and Conducting Chemically Derived Graphene Thin Films, *Advanced Functional Materials* 19(16) (2009) 2577-2583.

[17] R.J. Young, I.A. Kinloch, L. Gong, K.S. Novoselov, The mechanics of graphene nanocomposites: A review, *Composites Science and Technology* 72(12) (2012) 1459-1476.

[18] O.C. Compton, S. Kim, C. Pierre, J.M. Torkelson, S.T. Nguyen, Crumpled graphene nanosheets as highly effective barrier property enhancers, *Adv Mater* 22(42) (2010) 4759-63.

[19] W. Lee, J.U. Lee, B.M. Jung, J.-H. Byun, J.-W. Yi, S.-B. Lee, B.-S. Kim, Simultaneous enhancement of mechanical, electrical and thermal properties of

graphene oxide paper by embedding dopamine, Carbon 65 (2013) 296-304.

[20] B. Ramezanzadeh, M.H. Mohamadzadeh Moghadam, N. Shohani, M. Mahdavian, Effects of highly crystalline and conductive polyaniline/graphene oxide composites on the corrosion protection performance of a zinc-rich epoxy coating, Chemical Engineering Journal 320 (2017) 363-375.

[21] E.G. B. Ramezanzadeh, M. Mahdavian, E. Changizi, M.H. Mohamadzadeh Moghadam Covalently-grafted graphene oxide nanosheets to improve barrier and corrosion protection properties of polyurethane coatings, Carbon 93 (2015) 555-573.

[22] S.M. Kang, S. Park, D. Kim, S.Y. Park, R.S. Ruoff, H. Lee, Simultaneous Reduction and Surface Functionalization of Graphene Oxide by Mussel-Inspired Chemistry, Advanced Functional Materials 21(1) (2011) 108-112.

[23] X. Wan, Y. Zhan, Z. Long, G. Zeng, Y. He, Core@double-shell structured magnetic halloysite nanotube nano-hybrid as efficient recyclable adsorbent for methylene blue removal, Chemical Engineering Journal 330 (2017) 491-504.

[24] Z. Hu, Y. Huang, C. Zhang, L. Liu, J. Li, Y. Wang, Graphene-polydopamine-C60nanohybrid: an efficient protective agent for NO-induced cytotoxicity in rat pheochromocytoma cells, J. Mater. Chem. B 2(48) (2014) 8587-8597.

[25] L. Wang, D. Wang, Z. Dong, F. Zhang, J. Jin, Interface chemistry engineering for stable cycling of reduced GO/SnO<sub>2</sub> nanocomposites for lithium ion battery, Nano letters 13(4) (2013) 1711-6.

[26] L. Yang, S.L. Phua, J.K. Teo, C.L. Toh, S.K. Lau, J. Ma, X. Lu, A biomimetic

approach to enhancing interfacial interactions: polydopamine-coated clay as reinforcement for epoxy resin, *ACS applied materials & interfaces* 3(8) (2011) 3026-32.

[27] L. Zhang, M. Liu, S. Bi, L. Yang, S. Roy, X.Z. Tang, C. Mu, X. Hu, Polydopamine decoration on 3D graphene foam and its electromagnetic interference shielding properties, *J Colloid Interface Sci* 493 (2017) 327-333.

[28] E. Faure, E. Halusiak, F. Farina, N. Giambianco, C. Motte, M. Poelman, C. Archambeau, C. Van de Weerd, J. Martial, C. Jerome, A.S. Duwez, C. Detrembleur, Clay and DOPA containing polyelectrolyte multilayer film for imparting anticorrosion properties to galvanized steel, *Langmuir : the ACS journal of surfaces and colloids* 28(5) (2012) 2971-8.

[29] H. Wu, M.R. Kessler, Multifunctional Cyanate Ester Nanocomposites Reinforced by Hexagonal Boron Nitride after Noncovalent Biomimetic Functionalization, *ACS applied materials & interfaces* 7 (2015) 5915–5926.

[30] Sang-Ha Hwang, Dongwoo Kang, Rodney S. Ruoff, Hyeon Suk Shin, Y.-B. Park, Poly(vinyl alcohol) Reinforced and Toughened with Poly(dopamine)-Treated Graphene Oxide, and Its Use for Humidity Sensing, *ACS Nano* 8 (2014) 6739–6747.

[31] W. Xiao, P. Zhao, S. Deng, N. Zhang, Anchoring H3PW12O40 on 3-aminopropyltriethoxysilane modified graphene oxide: enhanced adsorption capacity and photocatalytic activity toward methyl orange, *New J. Chem.* 39(5) (2015) 3719-3727.

[32] I. Kaminska, M.R. Das, Y. Coffinier, J. Niedziolka-Jonsson, J. Sobczak, P. Woisel,

J. Lyskawa, M. Opallo, R. Boukherroub, S. Szunerits, Reduction and functionalization of graphene oxide sheets using biomimetic dopamine derivatives in one step, *ACS applied materials & interfaces* 4(2) (2012) 1016-20.

[33] Y. Zhan, X. Wan, S. He, Q. Yang, Y. He, Design of durable and efficient poly(arylene ether nitrile)/bioinspired polydopamine coated graphene oxide nanofibrous composite membrane for anionic dyes separation, *Chemical Engineering Journal* 333 (2018) 132-145.

[34] C. Wang, Y. Lan, W. Yu, X. Li, Y. Qian, H. Liu, Preparation of amino-functionalized graphene oxide/polyimide composite films with improved mechanical, thermal and hydrophobic properties, *Applied Surface Science* 362 (2016) 11-19.

[35] A.K. Das, M. Srivastav, R.K. Layek, M.E. Uddin, D. Jung, N.H. Kim, J.H. Lee, Iodide-mediated room temperature reduction of graphene oxide: a rapid chemical route for the synthesis of a bifunctional electrocatalyst, *J. Mater. Chem. A* 2(5) (2014) 1332-1340.

[36] S. Stankovich, D.A. Dikin, R.D. Piner, K.A. Kohlhaas, A. Kleinhammes, Y. Jia, Y. Wu, S.T. Nguyen, R.S. Ruoff, Synthesis of graphene-based nanosheets via chemical reduction of exfoliated graphite oxide, *Carbon* 45(7) (2007) 1558-1565.

[37] D. Zhong, Q. Yang, L. Guo, S. Dou, K. Liu, L. Jiang, Fusion of nacre, mussel, and lotus leaf: bio-inspired graphene composite paper with multifunctional integration, *Nanoscale* 5(13) (2013) 5758-64.

[38] Z. Wang, Y. Dong, H. Li, Z. Zhao, H.B. Wu, C. Hao, S. Liu, J. Qiu, X.W. Lou,

Enhancing lithium-sulphur battery performance by strongly binding the discharge products on amino-functionalized reduced graphene oxide, *Nat Commun* 5 (2014) 5002.

[39] F.M. Wenliang Tian, Li Liu, Ying Li, Fuhui Wang, The failure behaviour of a commercial highly pigmented epoxy coating under marine alternating hydrostatic pressure, *Progress in Organic Coatings* 82 (2015) 101-112.

[40] M.-Y. Jiang, L.-K. Wu, J.-M. Hu, J.-Q. Zhang, Silane-incorporated epoxy coatings on aluminum alloy (AA2024). Part 1: Improved corrosion performance, *Corrosion Science* 92 (2015) 118–126.

[41] B. Ramezanzadeh, S. Niroumandrad, A. Ahmadi, M. Mahdavian, M.H.M. Moghadam, Enhancement of barrier and corrosion protection performance of an epoxy coating through wet transfer of amino functionalized graphene oxide, *Corrosion Science* 103 (2016) 283-304.

[42] A.S. Castela, A.M. Simões, An impedance model for the estimation of water absorption in organic coatings. Part I: A linear dielectric mixture equation, *Corrosion Science* 45(8) (2003) 1631-1646.

**Highlights:**

- (1) The modification of the GO with PDA improves the compatibility between GO and EP.
- (2) EIS results show that the GO-PDA/EP has longer service life than blank EP.
- (3) SVET results imply that GO-PDA/EP with damages has better corrosion resistance.

ACCEPTED MANUSCRIPT